Manuscript

Cortical GABAergic inhibition dynamics around hippocampal sharp-wave ripples

Edris Rezaei[1], Setare Tohidi[1]

Author affiliations:

1. Canadian Centre for Behavioural Neuroscience, University of Lethbridge; Lethbridge, AB, T1K 3M4, Canada.

Corresponding author to: Edris Rezaei

Email: edris.rezaei@uleth.ca

Abstract

Cortical inhibition, mediated by GABA, is essential in balancing excitation and modulating neural processing, but it is unclear to what extent inhibitory dynamics are responsive to internally generated hippocampal activity, such as sharp-wave ripples (SWRs). Employing widefield imaging of extracellular GABA with iGABASnFR2 and hippocampal recordings, we characterized cortical inhibition during sleep–awake states and in the neighborhood of SWRs. Sleep–awake transitions drastically reorganized cortical levels of GABA, with increased inhibition in wakefulness and decreased upon entering NREM sleep. In the neighborhood of SWRs, inhibition was state- and region-specific: during NREM, medial cortices (e.g., retrosplenial) increased GABA before SWRs, whereas sensory areas in the lateral cortices decreased it; during wake, GABA increased in lateral cortices after SWRs. These findings reveal that cortical inhibition is not static and ubiquitous but instead is dynamically characterized by brain state, orchestrating the flow of hippocampal outputs to the rest of the cortex. Inhibitory modulation, as our data reveal, forms a mechanism allowing selective gating of memory-related activity during wakefulness and sleep.

Keywords: Cortical inhibition, GABA dynamics, Sharp-wave ripples, Brain state transitions, Hippocampal–cortical communication

Introduction

Cortical function is revealed as a balance of excitation and inhibition that together determines the dynamics of neural circuits and behavior [1]. Excitatory neurons produce the majority of the cortical output and communicate long distance between brain regions [2]. Such excitatory flow must be modulated to ensure stable network, accurate construction of information, and adaptive behavioral output [3]. Inhibitory interneurons, about 20–30% of the cortical neurons, govern circuit excitability, neuron responsiveness, as well as rhythmic network activity during brain states [4-5]. Of the inhibitory interneurons, three subtypes of GABA-releasing interneurons have been distinguished: parvalbumin-expressing (PV+), somatostatin-expressing (SST+), as well as vasoactive intestinal peptide-expressing (VIP+) interneurons [5-7]. PV+ interneurons that target the perisomatic of the pyramids are the fast spikers that contribute to feedforward inhibition [8]. Acting rapidly to turn down pyramidal activity with millisecond fidelity, they enhance temporal fidelity to maintain

gamma oscillation [9-10]. SST+ interneurons, on the other hand, innervate distal dendrites, acting feedback inhibition that reduces top-down as well as long-range integrative processing [11-13]. VIP+ interneurons, in turn, inhibit others of their kind, SST+ in particular, to recruit dis-inhibitory circuits to maintain pyramidal neuron output during behavioral demands such as attention or level of arousal change [14-16]. All in all, inhibition in no respect constitutes the easy opposite of excitation, but rather an operating mechanism that constrains computation by spatially and temporally distinctive control [1]. Inhibitory action chooses synaptic plasticity, tunes excitatory drive, and synchronizes distributed communication of cortical areas [6]. E/I balance dynamically varies in correspondence with sleep, wake, attention, and locomotion [17]. Inhibition disruption has been implicated in a broad spectrum of neuropsychiatric illnesses like epilepsy, autism spectrum disorder, and schizophrenia [18]. In this type of situation, it is preferable to have an idea of how cortical GABAergic inhibition is regulated by internally self-generated hippocampal activity patterns like sharp-wave ripples (SWRs), as they are indeed built to synchronize brain-wide communication in sleep as well as quiet wakefulness.

Recent studies have started to answer this question by describing excitatory cortical activity in response to hippocampal SWRs. A study using genetically encoded glutamate sensors indicated that cortical excitatory activity was strongly modulated by SWRs in a state-dependent manner. Karimi Abadchi et al. [19-20] demonstrated that, during NREM sleep, the SWRs precede a period of suppression in the whole cortex that is followed by sequential activation originating in medial and in visual cortices, areas involved in the default mode system. During quiet wakefulness, however, SWRs are followed by robust suppression in agranular retrosplenial cortex, with late rebound in cortical glutamatergic activity. These studies demonstrate that SWRs have organized and state-specific excitatory patterns of excitation as their outcome. Cortical computation, however, is almost never regulated by excitation in isolation. Since excitatory drive is generally followed or accompanied by inhibition [1,6], the state-dependent patterns of excitation during SWRs thus inevitably bring to the forefront the question of the corresponding inhibitory patterns. Thus, to this point, whereas excitatory responses have been accurately described, the inhibitory aspect of the cortical responses to SWRs has remained to a great extent uninvestigated. It is important to know how it is that GABAergic inhibition plays its part in this process, since the generation of the timing, spread, and functional significance of the cortical activation is controlled by the regulatory action of the inhibition mechanisms.

104 Here, we attempt to fill this gap; in the process, we combine widefield imaging of the genetically
105 encoded GABA sensor iGABASnFR2 [21] with hippocampal electrophysiology to track GABAergic
106 dynamics in the dorsal cortex during different states of the brain such as NREM, REM, and wake.
107 We first establish the baseline by describing the spontaneous cortical GABA transients during
108 these states, against which to gauge state-dependent GABAergic inhibition. We then inquired
109 whether SWRs shape cortical GABAergic inhibition in time- as opposed to space-ordered patterns,
110 as one would expect should hippocampal memory-related activity be selectively modulated by
111 distributed inhibitory processes. Emphasizing the inhibitory aspect of the cortical response to
112 SWRs, our study attempts to reveal a level of cortico-hippocampal organization that exists but
113 moves beyond the level of the excitatory to the level of the inhibitory circuits that defines the flow
114 of information across the brain.

115 **Materials and methods**

116 **Animals and experimental conditions**

117 We employed eight adult (>2 months) EMX-Cre female and male mice of the C57BL/6J strain for
118 imaging studies. For studying natural sleep, EMX-Cre mice were injected intracranially with AAV
119 vectors in a Cre-dependent manner to drive the expression of the genetically encoded GABA
120 sensor iGABASnFR2 in neocortical and hippocampal excitatory neurons. This enabled optical
121 reporting of extracellular GABA in excitatory cortical circuits. Strong expression of
122 iGABASnFR2 in targeted brain areas was validated through brain sectioning analysis as outlined
123 in our previous publication [22]. Mice were group-housed (two to five mice) under a 12-hour light-
124 dark cycle and had ad libitum access to water and a standard laboratory mouse diet. For sleep
125 recording studies, mice were singly housed after head-plate and electrode implantation surgery.
126 All animal studies were approved by the University of Lethbridge Animal Care Committee and
127 adhered to the Canadian Council for Animal Care guidelines.

128 **Viral constructs and retro-orbital injection procedure**

129 To enable selective detection of extracellular GABA dynamics in excitatory cortical circuits, we
130 used EMX-Cre transgenic mice, in which Cre recombinase is primarily expressed in excitatory
131 pyramidal neurons of the neocortex and hippocampus. This allowed for Cre-dependent expression

132 of genetically encoded sensors specifically in those neurons. Two AAV vectors were used:
133 AAV2/PHP.N-Syn-flex-iGABASnFR2, encoding the Cre-dependent GABA sensor, and
134 AAV2/PHP.N-Syn-flex-cpSFGFP, a non-sensing cytosolic GFP control. Both constructs were
135 obtained from the Canadian Neurophotonics Platform Viral Vector Core (RRID: SCR_016477)
136 and purified to a final concentration of 1.5×10^{13} genome copies per milliliter (GC mL^{-1}). Retro-
137 orbital injections [23]which outlines systemic delivery using the PHP.N capsid [24]. The animals were
138 anesthetized using isoflurane (maintained at 1.5–2%), and Metacam (5 mg/kg) was given by
139 subcutaneous. One drop of 0.5% proparacaine hydrochloride ophthalmic anesthetic was instilled
140 prior to injection. The 30-gauge needle was inserted at an angle of 30° into the medial canthus,
141 and 1.4×10^{11} GC of the viral vector was delivered into the retro-orbital sinus. This method allowed
142 widespread brain expression of iGABASnFR2 in excitatory neurons for the optical detection of
143 extracellular GABA in mesoscale imaging studies.

144 **Surgical procedure and electrophysiological recording setup**

145 The animals were given buprenorphine (0.05–0.1 mg/kg, subcutaneously) 30 minutes prior to
146 surgery, and then isoflurane (1–2% oxygen) was administered via a nose cone. The scalp was
147 shaved and sterilized, and the skull was covered with C&B Metabond (Parkell, Inc.), to which a
148 custom-designed headplate was attached over the skull. A 12-mm glass coverslip (Carolina
149 Biological Supply, Cat. No. 633005) was then cemented to establish a chronic cranial window to
150 image at the mesoscale. The LFP recordings were obtained through teflon-coated 50 µm stainless
151 steel wires (A-M Systems) implanted for electrophysiology. A bipolar electrode was positioned in
152 the right hippocampus through craniotomy at approximately 2.6 mm laterally from the midline,
153 tangent to the posterior edge of the occipital suture. The electrode was advanced at a 57° angle
154 relative to vertical while monitoring neural signals both visually and audibly. Once optimal signal
155 quality was achieved, the electrode was fixed in place using Krazy Glue and C&B Metabond. In
156 addition, a bipolar EMG electrode was implanted in the nuchal muscles to record muscle tone.
157 LFP signals from hippocampal electrode was amplified (×1,000), bandpass filtered (0.1–10,000
158 Hz) using a Grass A.C. pre-amplifier (Model P511, Artisan Technology Group), and digitized at
159 20 kHz using a Digidata 1440 acquisition system (Molecular Devices Inc.).

160 **Habituation for head-restraint sleep and wakefulness experiments**

They were then gradually introduced to the recording device after 14 days of recovery by positioning the animals on the recording platform. The first step consisted of letting the animals get to the platform and adapt to the environment. On subsequent days, having settled, they were positioned on head restraint in step increases in the period of head fixation, initiated at five minutes during the first day and incremented in five-minute increases to a period of one hour total.

GABA imaging during wakefulness

Following the habituation, every animal was recorded every three days, with three to four sessions being done on each mouse. The recording was always done at the same time of the day to reduce variability and stress. Finally, the animals were put back into their home cages in the housing pod, where they rested and recovered before the subsequent recording.

GABA imaging during natural sleep

Sleep recordings were performed after the completion of all wakefulness sessions. To optimize conditions for natural sleep under head restraint, the day before recording, the animals were moved from their home cage in the colony room to a separate room at noon. Sleep was restricted to ~6 hours by gently stimulating the mice with a cotton-tip stick whenever they showed signs of drowsiness. The animals were then transferred to a larger cage containing new objects, such as a running wheel, Cheerios, and a water container, and left in surgical recovery where the temperature was controlled. The next day, the animals were transferred to the imaging room, and sleep recordings began at ~7:00 AM. Once recording finished, the animals were returned to their home cages in the podding room and allowed to sleep freely for at least three days before repeating the procedure for another recording.

GABA imaging

Imaging was undertaken with a custom macroscope comprising a front-to-front video lens setup, 8.6 × 8.6 mm field of view. The focal plane was set ~0.5–1 mm below the cortical surface. Fluorescence signals were recorded with a 12-bit CCD camera (1M60 Pantera, Dalsa, Waterloo, ON) attached to an EPIX E8 frame grabber and operated by XCAP 3.8 software (EPIX, Inc.,

Buffalo Grove, IL), imaging at a frame rate of 80 Hz. Imaging parameters have been used in previous studies, including voltage-sensitive dye imaging [25-27]. Sequential illumination was provided using alternating blue (473 nm) and green (530 nm) LEDs (Thorlabs) [28]. Blue light (473 nm, filtered through a 467–499 nm bandpass) was employed to excite the iGABASnFR2 indicator, and green light (530 nm, filtered through a 527/42 nm bandpass) for intrinsic signal imaging of blood volume. A bandpass emission filter was placed in front of the CCD camera to facilitate selective detection of either fluorescence or reflectance signals. Blue and green light-emitting diodes (LEDs) were used as illumination sources. They were alternatively synchronized and frame-by-frame, utilizing transistor–transitor logic (TTL) triggering, to offer temporal control precisely so as to interleave acquisitions of reflectance and fluorescence images at 40 Hz per channel. Reflectance images, which may be used for corrections of blood artifacts [29-31], were analyzed as well within our current pipeline.

Preprocessing

Image data were transferred into MATLAB; blue and green frames were differentiated based on reference frames to set up illumination origins. Only the region of interest (ROI) was selected utilizing a binary mask. Slow baseline drifts were eliminated utilizing a local detrending algorithm, based on a filter of the Chebyshev type. The ratio of $\Delta F/F_0$ was normalized to the fluorescence signals (F) based on the following formula: $\Delta F/F_0 = (F - F_0) / F_0 \times 100$, where the detrended curve provided an estimate of F_0. To filter out high frequency noise, a low-pass finite impulse response (FIR) filter, utilizing a 6 Hz cut-off, was used on the time series of $\Delta F/F_0$. Hemodynamic artifacts in the blue channel were corrected by linear regression, using the green reflectance signal as a regressor. To denoise the data further, singular value decomposition (SVD) was applied to the corrected blue channel, and the first 300 components were used for reconstruction.

Sleep scoring

Motion data were obtained from behavior camera (frame rate = 25HZ) by the FaceMap [32], which computes frame-to-frame pixel intensity differences in manually defined regions of interest (ROIs). Five ROIs—nose, whisker pad, ear, shoulder, and trunk—were selected to monitor both subtle facial expressions and body movement. Motion signals were time-locked to electrophysiological recordings. Wakefulness in this study was identified by clear motor activity in video recordings and high EMG amplitude. NREM sleep was determined by decreased EMG tone, low hippocampal

217 theta-to-delta power ratio, and the occurrence of large irregular activity in the hippocampal LFP.
218 REM sleep was characterized by EMG suppression, sustained hippocampal theta oscillations, and
219 high theta-to-delta ratios.

220 **SWR detection**

221 SWRs were determined on the basis of a modified Karimi Abadchi et al [20] protocol. The raw LFP
222 signals of the hippocampus were initially down-sampled at 2 kHz and band-filtered between 110
223 to 250 Hz (ripple band) on a real-valued MATLAB (MathWorks) Morlet wavelet. The ripple-band
224 signal was then rectified and smoothed. screened SWRs were detected when ripple power crossed
225 above a threshold set as the mean plus a multiple of the standard deviation of the baseline. The
226 multiplier was set for each animal to compensate for inter-individual differences in signal quality.
227 Onset and offset times were set using a second threshold of 75% of the detection threshold. In
228 order to further refine event detection, only those SWRs with an appropriate duration were kept.
229 For each event window, event center was defined as the time of the greatest negative deflection
230 (trough) of the ripple-band sound. Events within 50 ms of an event were grouped into one SWR.

231 **Normalization of peri-SWR neocortical activity using Z-scoring**

232 To normalize peri-SWR neocortical GABA activity, random timestamps were created by
233 shufflings of the inter-SWR intervals within individual recording sessions. Imaging stacks 0.5
234 seconds before and 0.5 seconds after the timestamp were sampled and time-aligned for each
235 random event. Averaging peri-event stacks across all random timestamps were then calculated to
236 compute a baseline mean stack, as well as a parallel SD stack for standard deviation. These mean
237 and SD stacks served as references to z-score normalization. The peri-SWR imaging stacks were
238 then all normalized by subtraction of the baseline mean stack and division by the SD stack on a
239 pixel-by-pixel basis to provide a z-scored representation of neocortical activity.

240 **Statistical Analysis**

241 All statistical analyses were conducted using built-in functions in MATLAB.

Data availability

All data and custom software/algorithms necessary to interpret and replicate the findings and methods of this article are available upon request.

Results

Experimental protocol for investigating neocortical GABA dynamics

We retro-orbitally injected AAV2/PHP.N-Syn-Flex-iGABASnFR2 or control construct (cpSFGFP) into animals (see Figure 1A). The configuration of our recording involved mesoscale GABA imaging, in-vivo electrophysiological recordings, and monitoring of behavior (see Figure 1B). Protocols of imaging were conducted at 80 Hz cycling blue (470 nm) and green (530 nm) LEDs alternating with a CCD camera. LFPs were recorded from the right dorsal CA1 to study hippocampal sharp-wave ripples (SWRs), with neck EMG and a camera for monitoring behavior. A schematic of the headplate placement and the 17 cortical regions imaged in the right hemisphere is shown in **Figure 1Ci–ii**. Example cortical images are shown in Figure **1Ciii–iv**, with the dorsal retrosplenial cortex (dRSC) marked as a representative region of interest (ROI). To correct for hemodynamic artifacts, GABA fluorescence signals were normalized to simultaneously recorded reflectance traces (**Figure 1Cv–vi**).

Frames of images were registered to the center of SWR activity (see Figure 1Di), averaged and concatenated into single peri-ripple montages (see Figure 1Di–ii). To reveal cortical GABAergic inhibition dynamics, we provide two companion videos. **Video 1** provides spontaneous neocortical GABA dynamics during wakefulness, as $\Delta F/F_0$ signals via iGABASnFR2, together with hippocampal local field potential (LFP) and electromyography (EMG) traces verifying wakefulness. **Video 2** illustrates the multimodal sleep-scoring method, in combination of hippocampal ripple-band power, EMG power, raw EMG traces, pupil diameter, as verified in synchronized infrared video, to distinguish wakefulness, non-rapid eye movement (NREM) sleep, and rapid eye movement (REM) sleep.

Cortical GABA Dynamics Across Sleep-Wake State Transitions

To examine the spatiotemporal dynamics of neocortical GABA activity in state transitions, we unilaterally imaged fluorescence signals from the GABA-sensing reporter iGABASnFR2 by widefield imaging. Representative spatial montages and time series traces were analyzed to

evaluate GABA dynamics between cortical regions during transitions from NREM to wakefulness and wakefulness to NREM sleep.

NREM to awake Transition

Figure 2Ai represents spatial montages of neocortical GABA activity at transition to wake (**Video 3**) with overall increases in fluorescence signal (z-scored ΔF/F) on transition, indicative of increased levels of extracellular GABA. The phenomenon is quantified further in (**Figure 2Aii**), which reveals regions such as V1, RSC2, and FLS1 exhibit a ramp-like build-up of GABA activity begun several seconds before transition and peaking a short time after wake onset. **Figure S1iii** validates the same in coherence spectra in increased inter-regional synchrony for delta and low-theta bands on transition, and in functional connectivity (**Figure S2iv**), which similarly reveals a transition from robust, spatially localized correlations in NREM to a global one in wake. The right-most difference matrix reveals increased correlation of frontal and posterior cortices on transition.

Wake to NREM Transition

At wake-to-NREM transition (**Figure 2Bi**), spatial montages reveal a prominent reduction of GABA fluorescence across the neocortex (**Video 4**). Time series traces in (**Figure 2Bii**) from the same three areas exhibit a progressive decline in activity, starting approximately 5 seconds prior to transition and persisting into early NREM. In parallel, **Figure S1i** reveals that there is increased coherence in lower frequencies when entering NREM, pointing to more synchronous slow oscillatory dynamics. Functional connectivity (**Figure S2iii**) confirms stronger localized correlations in NREM relative to the more diffuse patterns of wake. The difference matrix reveals increased correlation specifically in posterior and somatomotor areas.

NREM to REM Transition

Figure 3Ai depicts the spatial dynamics of GABA activity in NREM to REM transitions (**Video 5**). GABA activity seemed more spatially diverse than in other transitions, with some areas showing transient increases and others remaining stable. Time series in **Figure 3Aii** indicate a modest, transient increase in GABA levels in all three regions, followed by gradual suppression throughout the REM episode. Coherence spectra in **Figure S1iv** show a decrease in inter-regional synchrony in REM as compared to NREM. This is also reflected in the functional connectivity heatmaps in **Figure S2ii**, which illustrate a general weakening of correlation patterns in REM. The

difference matrix indicates subtle reductions in cortical synchrony especially in posterior and medial areas.

REM to Wake Transition

As illustrated in **Figure 3Bi**, the REM-to-wake transition (**Video 6**) is characterized by a trough in GABA signal at the time of transition, followed by an abrupt rebound. The time courses of **Figure 3Bii** indicate this transient inhibition most prominently in V1 and FLS1, and thus also indicate a transient phase of disinhibition during transitioning out of REM. **Figure S1ii** indicates wake-on transitions out of REM involve increases in coherence, particularly in delta and low-theta frequencies, which would be consistent with reorganization into wakeful dynamics. Consistent with this, the difference connectivity matrix of **Figure S2i** indicates heightened inter-regional correlations following REM, particularly in anterior sensory-motor regions.

State-dependent spatiotemporal patterns of cortical inhibition around sharp-wave ripples

Studies have shown that sharp-wave ripples (SWRs) mediate communication between the hippocampus and cortex in offline brain states, such as sleep and quiet wakefulness [33-37]. It has been shown that the disruption of SWRs impairs memory consolidation, thus demonstrating their functional importance [38-39]. These events represent an excellent portal for investigating localized, temporally specific manipulation of cortical GABAergic inhibition. Following this background, we next addressed the question of how neocortical GABAergic inhibition responds to SWRs events. Using the iGABASnFR2 sensor, we combined unilateral imaging of neocortical extracellular GABA with local field potential (LFP) recordings from CA1 pyramidal cells to study the spatiotemporal features of extracellular GABA dynamics across the dorsal cortex in relation to hippocampal sharp-wave ripples (SWRs) in natural sleep and wakefulness.

Montages of **Figure 4A**, reveal neocortical GABA's temporal and spatial pattern across different states of the brain. Importantly, in time with NREM sleep (**Figure 4Ai**) neocortical GABA activation began relatively early (**Video 7**), at approximately 150 ms before the SWR center (t = 0). The activation peaked in retrosplenial cortex (RSC) and occurred before the SWR center (**Figure 4Bi**). The temporal profile of the activation was medial-to-lateral in direction, and medial parts of the brain like the RSC exhibited earliest and greatest activation. Besides strong activation, a clear GABA deactivation pattern was seen in lateral areas before the SWR center. These

observations lead us to speculate on the broader significance of GABAergic signaling in sleep and wakefulness. Conversely, during wakefulness (**Figure 4Aii**), no initial GABA activation was observed (**Video 8**). Rather, extracellular GABA activity within neocortical areas slowly built up following the SWR center (t = 0), peaking ~ 500 ms after SWR (Figure 4Biii–iv).

Interestingly, wakefulness activation evolved in lateral-to-medial sequence, initiating in visual and somatosensory cortices regions and spreading to medial regions. Deactivation of wakefulness was much less strong and little suppression took place across regions before the SWR center, which gave extra support to the state-dependent difference in the GABA modulation.

To explore the spatial organization of peri-SWR GABA activity in more depth, we examined four major neocortical subnetworks: medial, visual, auditory, and somatomotor—as outlined in **Figure 4Ci**. Amplitude of activation were determined by taking mean of the complete signal in whole full width at half-maximum (from t_1 to t_2), as in **Figure 4Cii**. Repeated measures ANOVA confirmed sub-network-based effects for wakefulness and NREM. In wakefulness (**Figure 4Civ)**, ANOVA results showed significant subnetwork effect ($F(3,18) = 30.051$, $p = 3.18 \times 10^{-5}$; Greenhouse-Geisser adjusted $p = 7.03 \times 10^{-5}$). Follow-up post-hoc analyses verified medial subnetwork had highest activation amplitudes, which were higher comparing to auditory ($p = 0.0075$) and somatomotor ($p = 0.0027$) subnetworks. The visual subnetwork had higher activation amplitudes comparing to auditory ($p = 0.0025$) and somatomotor ($p = 0.0053$) subnetworks. Second, in NREM (**Figure 4Cv**), the sub-network based effect attained significance ($F(3,12) = 21.608$, $p = 3.96 \times 10^{-5}$, Greenhouse-Geisser adjusted $p = 0.0017$). Follow-up post-hoc analyses verified medial subnetwork had highest activation, which was statistically significant comparing to auditory ($p = 0.0305$) and somatomotor ($p = 0.0366$) subnetworks. The visual subnetwork had intermediate activation, and its amplitudes were higher comparing to auditory ($p = 0.0146$) and somatomotor ($p = 0.0366$) subnetworks.

Amplitudes of deactivation (**Figure 3D**) were explored and were found to exhibit state- and specific patterns during wakefulness and NREM. During wakefulness (**Figure 4Di**), the deactivations were attenuated but had robust subnetwork effects ($F(3,12) = 13.869$, $p = 0.00033$, Greenhouse-Geisser adjusted $p = 0.0047$). The post-testing indicated that auditory subnetwork had less deactivation compared to visual ($p = 0.032$) and medial ($p = 0.041$) subnetworks. The visual subnetwork had greater deactivation than the somatomotor ($p = 0.061$) subnetwork. During NREM (**Figure 4Dii**), deactivation amplitudes were significantly larger, with repeated measures ANOVA indicating a strong subnetwork effect ($F(3,12) = 21.608$, $p = 3.96 \times 10^{-5}$; Greenhouse-Geisser

corrected $p = 0.0017$). Post hoc tests indicated significant differences between the auditory and visual ($p = 0.015$), auditory and medial ($p = 0.031$), and somatomotor and visual ($p = 0.010$) subnetworks.

To investigate state-dependent modulation more deeply, we recorded amplitudes of GABA activation and deactivation in different neocortical regions during wakefulness and sleep (**Figure S3A**). Activation and deactivation were comparable across states, as confirmed by correlation analyses (**Figure S3B**). Moreover, the comparisons of activation and deactivation amplitude at the subnetwork-specific levels discovered no statistically significant differences between NREM and wakefulness, again highlighting unique modulation profiles for both states (**Figure S3C**). **Activation Amplitudes:** A mixed repeated-measures ANOVA revealed a significant main effect of state on activation amplitudes ($F(1,10) = 28.266$, $p = 0.00034$), with NREM sleep exhibiting higher overall amplitudes. Subnetwork effects were also significant across states ($F(3,30) = 51.895$, $p = 5.50 \times 10^{-12}$), indicating robust differences among regions. However, the interaction between state and subnetwork was not significant ($F(3,30) = 1.605$, $p = 0.209$), suggesting that the relative differences among subnetworks were preserved across states. **Deactivation Amplitudes:** Similarly, for deactivation amplitudes, a mixed repeated-measures ANOVA showed a significant main effect of state ($F(1,8) = 18.571$, $p = 0.0026$), with NREM showing stronger deactivation than wakefulness. Subnetwork effects were again significant ($F(3,24) = 35.134$, $p = 6.08 \times 10^{-9}$), while the interaction between state and subnetwork was not significant ($F(3,24) = 1.686$, $p = 0.197$), indicating that subnetwork-specific patterns remained consistent across brain states.

Temporal mapping of cortical GABA peaks reveals brain-state-dependent propagation during SWRs

We then investigated the temporal profile of peak GABA activation across cortical areas. The time of peak neocortical GABA activation (t_p) was approximated, as the time of peak GABA signaling from the center of the SWR (**Figure 5Ai**), to measure the spatiotemporal extent of inhibition in SWRs in NREM sleep and wakefulness. t_p values in NREM sleep were highly regionally heterogeneous (**Figure 5Aii**), as confirmed by repeated-measures ANOVA ($F(10,40) = 5.0973$, $p = 8.91 \times 10^{5}$). Analysis of linear trends showed a weak but significant medial-to-lateral gradient in the time profile of activation (slope = 0.0113 s/region, $p = 0.047$). Spatial maps (**Figure 5Av**) showed the trend, with medial regions like RSC1 and RSC2 with earlier activation than the later

activation of lateral cortices. In wakefulness, t_p values had increased and more organized regional heterogeneity (**Figure 5Aiii**), and signification effect confirmed by repeated-measures ANOVA ($F(10,60) = 20.156$, $p = 1.12 \times 10^{15}$). The linear trend discovered was stronger (slope = 0.0272 s/region, $p = 0.024$), and representative of a greater medial-to-lateral gradient.

Spatial maps (**Figure 5Avi**) confirmed this reversal of patterns: medial regions had later peak GABA activation compared to lateral regions. Line-by-line comparison of trend slopes between brain states (**Figure 5Aiv**) identified that the medial-to-lateral gradient was much greater during wake than during NREM. In aggregate, these results define a state-dependent reorganization of peak neocortical GABA timing: gradual and subtle during NREM sleep, but more sudden and orderly during wakefulness. We compared rise times of extracellular GABA signals between regions and states (**Figure S4A**). Rise times were similar in all cases, so variation in t_p found is better ascribed to differences in timing, as opposed to in speed of activation. In addition, in wakefulness,.t_p values were positively correlated ($r = 0.558$, $p = 0.011$; **Figure S4Bii**) with lateral cortical location, as would be expected for a lateral-to- medial propagation of GABA activation. In NREM sleep, however, there was a significant negative correlation ($r = –0.391$, $p = 0.040$; **Figure S4Biii**), indicative of medial regions' earlier activation. These results lend further support to a state-dependent reorganization of spatiotemporal characteristics of neocortical GABAergic signaling during hippocampal SWRs.

Spatial and temporal modes of peri-ripple iGABASnFR2 activity and region-specific dynamics

We then examined if ripple-related neocortical GABA dynamics show unique spatial motifs and temporal structures at the network level. To decompose spatiotemporal neocortical GABA activity into general spatial and temporal structures, we applied singular value decomposition (SVD) to GABA signals close to SWRs **(Figure 6A, B**). Component 1 mapped diffuse activation of GABA (Components 1i), and the corresponding temporal trace (Component 1ii) consisted of a punctuate onset of extracellular GABA at ripple onset ($t = 0$). Components 2–5, on the other hand, detected state-specific characteristics. In wakefulness (**Figure 6A**), spatial maps (Components 2–5i) illustrated regionally localized activation of GABA in lateral regions, but corresponding temporal traces (Components 2–5ii) contained transient, fast features, suggesting fast, region-specific inhibition. In NREM sleep (**Figure 6B**), higher-order spatial components detected heightened

426 recruitment of medial regions, including the retrosplenial cortex (RSC). The temporal components
427 in NREM were slow and less well time-locked to onset of ripples compared to wakefulness. We
428 also reconstructed neocortical GABA activity in the neocortex close to SWRs in five representative
429 neocortical locations: RSC, BC, V1, auditory cortex (AUD), and forelimb somatosensory cortex
430 (FLS1) (**Figure 6C, D**). Under wakefulness (**Figure 6C**), BC and V1 had sharp, high-amplitude
431 GABA transients (**Figure 6Cii**), and statistical comparisons revealed heightened GABA responses
432 in sensory areas compared to the RSC (**Figure 6Ciii**). During NREM sleep (**Figure 6D**), RSC has
433 the strongest activation (**Figure 6Dii–iii**). Combined, these results show that while a global
434 elevation of inhibitory tone accompanies hippocampal ripples in both brain states, fine-scale
435 spatiotemporal patterns of neocortical GABA dynamics depend on brain state. Wakefulness
436 involves rapid, GABA activation in lateral sensory cortices, while NREM sleep recruits more
437 widespread, slower inhibitory responses with a focus on medial areas.

438 **Discussion**

439 **Summary of the Study**

440 In this study, we investigated how neocortical GABAergic inhibition is temporally and spatially
441 organized around internally generated hippocampal sharp-wave ripples (SWRs) across behavioral
442 states. Using mesoscale imaging of extracellular GABA with the iGABASnFR2 sensor alongside
443 simultaneous recordings of CA1 pyramidal neuron activity, we first characterized GABAergic
444 activity during spontaneous transitions between sleep and wakefulness. Next, we explored
445 spatiotemporal dynamics of neocortical GABA around hippocampal SWRs and found that cortical
446 GABAergic inhibition is spatially structured, exhibits propagating dynamics, and is strongly
447 modulated by brain state. Our results revealed distinct patterns of neocortical GABA dynamics
448 around SWRs , with medial-to-lateral propagation during NREM sleep and lateral-to-medial
449 propagation during wakefulness. Our results suggest that cortical GABAergic inhibition is actively
450 modulated by hippocampal output, and that this modulation differs across cortical subnetworks
451 and vigilance states.

452 To examine how GABAergic inhibition in the cortex is regulated by hippocampal sharp-wave
453 ripples (SWRs), we employed the genetically encoded GABA sensor iGABASnFR2, allowing
454 direct optical imaging of extracellular GABA dynamics in vivo [21]. We wanted to quantify
455 GABAergic inhibition across the whole dorsal cortex and thus conducted widefield imaging

through a large cranial window over the right hemisphere. To record hippocampal output in parallel, we measured local field potentials from the ipsilateral dorsal hippocampus. This unilateral approach was informed by previous reports of strong interhemispheric synchrony in both neocortical activity [40] and hippocampal SWRs [33,37], which made it adequate to describe ripple-cortical interactions. This setup enabled us to integrate mesoscale imaging with exact electrophysiological timing to investigate inhibitory dynamics during natural sleep and wakefulness at high spatial and temporal resolution.

Cortical GABA Dynamics During State transitions

First, we examined the changes in cortical GABA levels that take place during spontaneous behavior state transitions, and we complemented this analysis with coherence and correlation-based network methods to reveal their implications at the circuit level. As the brain transitioned from NREM sleep to wakefulness, we observed a dramatic increase in GABA activity, which was replicated across different cortical areas (**Figure 2Ai–ii**), and increased inter-areal coherence and functional connectivity (**Figures S1iii, S2iv**). This increase in inhibitory tone, coupled with increased synchrony, can reflect an active gating or stabilization process during the arousal process, promoting the coordination of sensory and motor pathways as the brain prepares for the state of behavioral responsiveness [41-43]. In contrast, transitions from wakefulness to NREM sleep were correlated with a decrease in extracellular GABA (**Figure 2Bi–ii**), together with increases in slow-frequency coherence (**Figure S1i**) and more tightly localized functional correlations (Figure S2iii). These are likely to represent a switch from fast, phasic inhibitory mechanisms to slower, synchronous, oscillatory modes typical of NREM sleep [44-45], in favor of the commencement of cortical downscaling and memory consolidation.

The dynamics of GABA in the neocortex across transitions involving REM sleep showed increasingly complex and varied dynamics. The transition from NREM to REM sleep was marked by modest, regionally specific increases in GABA levels, which were then followed by suppression (**Figure 3Ai–ii**). This transition also showed a decrease in coherence and weakening of inter-areal correlations (**Figures S1iv, S2ii**), consistent with the decoupled cortical dynamics characteristic of REM sleep. In contrast, the transition from REM sleep to wakefulness showed a large drop in GABA at the point of awakening (**Figure 3Bi–ii**), followed by rapid re-engagement, reflecting a brief release from inhibitory control [46-49]. This transition was accompanied by a large increase in coherence and correlation strength (**Figures S1ii, S2i**), marking a reorganization of network

synchrony required for cognitive and sensory engagement in wakefulness. Together, these findings highlight the dynamic and state-specific regulation of GABAergic tone across the neocortex, indicating that changes in inhibitory signaling are closely intertwined with macroscale network reconfiguration across sleep-wake transitions.

Ripple-triggered GABA responses are brain-state dependent

Past research with iGluSnFR has established that hippocampal SWRs are coordinated by state-dependent cortical excitation [19-20]. Our results build on this research by demonstrating that cortical inhibition, as assayed by the extracellular GABA imaging, is also state-dependently coordinated on SWRs. During NREM sleep, we found that extracellular GABA levels increased starting before ripple onset in medial cortical areas, including the retrosplenial cortex. This result is consistent with past work showing that SWRs recruit retrosplenial inhibitory neurons to fire during slow-wave sleep 50 and aligns with prior research on retrosplenial–hippocampal coordination during memory-related processing [51-52]. This initial medial activation was joined by a simultaneous deactivation in lateral sensory cortices, implicating a topographically organized inhibition pattern. By contrast, during wakefulness, GABAergic activity increased in primarily lateral cortical areas after ripple onset, whereas medial areas showed delayed or reduced responses. These findings together demonstrate that SWRs recruit not just excitatory but also inhibitory cortical networks in a temporally and spatially coordinated fashion, and that the organization of this recruitment is radically different in sleep versus wakefulness.

Temporal gradients reveal propagation of inhibitory signals

Time-to-peak (t_p) of neocortical GABA dynamics throughout different cortical areas showed medial-to-lateral propagation during NREM sleep, consistent with glutamate dynamics [19] and memory-related information flow direction between default-mode network structures. During wakefulness, direction of propagation was reversed, and propagation went from lateral to medial cortical compartments. These results are in concert with the suggestion that cortical inhibition characteristically follows excitation with a characteristic temporal delay [1,53,54] Neocortical inhibition in this case can function as a state-dependent gate of the hippocampal output, orchestrating temporally the inhibition control with the current sensory or cognitive demands. Directional asymmetry of propagation patterns uncovers the cortex to rescale not only the strength but also the spatiotemporal organization of inhibition in accordance with internal state.

517

518 **SVD reveals global vs. local components of ripple-evoked inhibition**

519 Our SVD characterization of neocortical GABA signals in hippocampal SWRs revealed typical
520 spatial and temporal patterns of inhibition. The first factor described a global increase in GABA
521 activity throughout the cortex that could be a generalized and synchronized inhibitory response
522 potentially used to suppress cortical excitability and runaway excitation in the progression of
523 memory-related hippocampal activity. Beyond this, components 2-5 represented more localized
524 and state-dependent dynamics. When awake, these components identified fast, transient increases
525 in GABA activity in mostly lateral cortical regions, which may represent regionally selective
526 gating of sensory information or circuit inhibition. During NREM sleep, GABA activity exhibited
527 wider and more sustained increases in medial regions, including the RSC, a region highly
528 interconnected with the hippocampus and involved in memory consolidation processes [35,46]. These
529 results indicate that SWR-evoked GABAergic inhibition is not homogeneous throughout the
530 cortex but rather consists of a global inhibitory scaffold with overlaid state-specific, spatially
531 directed components that can facilitate the routing and integration of memory-related information
532 during sleep and wakefulness.

533 **Conclusion**

534 In the current study, mesoscale imaging of iGABASnFR2 was used to map the dynamics of
535 extracellular GABA over the dorsal cortex during sleep-wake transitions and in response to
536 hippocampal sharp-wave ripples. The results show that cortical GABAergic inhibition is spatially
537 patterned and under strong control of behavioral states, suggesting that neocortical GABA
538 dynamics play an active role in the routing and filtering of memory-related outputs from the
539 hippocampus. While our imaging approach provides high temporal and spatial resolution over
540 large cortical areas, it remains nonspecific with regard to cell types and depth resolution. Therefore,
541 it would not be possible to distinguish between the behaviors of PV+, SST+, or VIP+ interneurons,
542 or clarify the inhibitory roles at the subcortical level. To further define the circuit mechanisms
543 underlying state-dependent and ripple-dependent inhibition, future studies employing
544 iGABASnFR2 in conjunction with optogenetic manipulation, cell-type-specific marker labeling,
545 or multiphoton microscopy will be necessary. In addition With recent advances in genetically
546 encoded sensors, it is now possible to simultaneously measure excitation and inhibition in vivo.

Combining iGABASnFR2 with glutamate sensors will enable direct assessment of excitation–inhibition balance in both healthy and disease models, offering new insights into how this balance is altered in disorders such as epilepsy or schizophrenia.

Acknowledgements

We thank Di Shao and the Animal Welfare Committee at the University of Lethbridge for their support in enabling the animal experiments. We also thank Majid H. Mohajerani for providing access to laboratory resources and equipment during the data collection phase of this project.

Funding

The author(s) declare that financial support was received for the research, authorship, and/or publication of this article. This work was supported by Alberta Innovate and Natural Sciences and Engineering Research Council of Canada (grant 390930), awarded to Majid H. Mohajerani.

Author contributions

E.R. conceptualized the study, and E.R. performed the experiments. E.R. and S.T. analyzed the data. E.R. wrote the manuscript and prepared figures.

Competing interests

The authors declare no competing interests.

Supplementary material

Supplementary material and methods are available .

565 **References**

566 1. Isaacson, J. S., & Scanziani, M. (2011). How inhibition shapes cortical activity. *Neuron,*
567 *72*(2), 231–243. https://doi.org/10.1016/j.neuron.2011.09.027
568 2. Harris, K. D., & Shepherd, G. M. G. (2015). The neocortical circuit: Themes and
569 variations. *Nature Neuroscience, 18*(2), 170–181. https://doi.org/10.1038/nn.3917
570 3. Haider, B., & McCormick, D. A. (2009). Rapid neocortical dynamics: Cellular and
571 network mechanisms. *Neuron, 62*(2), 171–189.
572 https://doi.org/10.1016/j.neuron.2009.04.008
573 4. Markram, H., Toledo-Rodriguez, M., Wang, Y., Gupta, A., Silberberg, G., & Wu, C.
574 (2004). Interneurons of the neocortical inhibitory system. *Nature Reviews Neuroscience,*
575 *5*(10), 793–807. https://doi.org/10.1038/nrn1519
576 5. Rudy, B., Fishell, G., Lee, S., & Hjerling-Leffler, J. (2011). Three groups of interneurons
577 account for nearly 100% of neocortical GABAergic neurons. *Developmental*
578 *Neurobiology, 71*(1), 45–61. https://doi.org/10.1002/dneu.20853
579 6. Tremblay, R., Lee, S., & Rudy, B. (2016). GABAergic interneurons in the neocortex:
580 From cellular properties to circuits. *Neuron, 91*(2), 260–292.
581 https://doi.org/10.1016/j.neuron.2016.06.033
582 7. Kepecs, A., & Fishell, G. (2014). Interneuron cell types are fit to function. *Nature,*
583 *505*(7483), 318–326. https://doi.org/10.1038/nature12983
584 8. Hu, H., Gan, J., & Jonas, P. (2014). Interneurons. Fast-spiking, parvalbumin^{+} GABAergic
585 interneurons: From cellular design to microcircuit function. *Science, 345*(6196),
586 1255263. https://doi.org/10.1126/science.1255263
587 9. Pouille, F., & Scanziani, M. (2001). Enforcement of temporal fidelity in pyramidal cells
588 by somatic feed-forward inhibition. *Science, 293*(5532), 1159–1163.
589 https://doi.org/10.1126/science.1060342
590 10. Bartos, M., Vida, I., & Jonas, P. (2007). Synaptic mechanisms of synchronized gamma
591 oscillations in inhibitory interneuron networks. *Nature Reviews Neuroscience, 8*(1), 45–
592 56. https://doi.org/10.1038/nrn2044
593 11. Silberberg, G., & Markram, H. (2007). Disynaptic inhibition between neocortical
594 pyramidal cells mediated by Martinotti cells. *Neuron, 53*(5), 735–746.
595 https://doi.org/10.1016/j.neuron.2007.02.012

12. Urban-Ciecko, J., & Barth, A. L. (2016). Somatostatin-expressing neurons in cortical networks. *Nature Reviews Neuroscience, 17*(7), 401–409. https://doi.org/10.1038/nrn.2016.53
13. Murayama, M., Pérez-Garci, E., Nevian, T., Bock, T., Senn, W., & Larkum, M. E. (2009). Dendritic encoding of sensory stimuli controlled by deep cortical interneurons. *Nature, 457*(7233), 1137–1141. https://doi.org/10.1038/nature07663
14. Pi, H.-J., Hangya, B., Kvitsiani, D., Sanders, J. I., Huang, Z. J., & Kepecs, A. (2013). Cortical interneurons that specialize in disinhibitory control. *Nature, 503*(7477), 521–524. https://doi.org/10.1038/nature12676
15. Lee, S., Kruglikov, I., Huang, Z. J., Fishell, G., & Rudy, B. (2013). A disinhibitory circuit mediates motor integration in the somatosensory cortex. *Nature Neuroscience, 16*(11), 1662–1670. https://doi.org/10.1038/nn.3544
16. Fu, Y., Tucciarone, J. M., Espinosa, J. S., Sheng, N., Darcy, D. P., Nicoll, R. A., Huang, Z. J., & Stryker, M. P. (2014). A cortical circuit for gain control by behavioral state. *Cell, 156*(6), 1139–1152. https://doi.org/10.1016/j.cell.2014.01.050
17. McGinley, M. J., Vinck, M., Reimer, J., Batista-Brito, R., Zagha, E., Cadwell, C. R., Tolias, A. S., Cardin, J. A., & McCormick, D. A. (2015). Waking state: Rapid variations modulate neural and behavioral responses. *Neuron, 87*(6), 1143–1161. https://doi.org/10.1016/j.neuron.2015.09.012
18. Marín, O. (2012). Interneuron dysfunction in psychiatric disorders. *Nature Reviews Neuroscience, 13*(2), 107–120. https://doi.org/10.1038/nrn3155
19. Karimi Abadchi, J., Nazari-Ahangarkolaee, M., Gattas, S., Bermudez-Contreras, E., Luczak, A., McNaughton, B. L., & Mohajerani, M. H. (2020, March 13). Spatiotemporal patterns of neocortical activity around hippocampal sharp-wave ripples. *eLife, 9*, e51972. https://doi.org/10.7554/eLife.51972
20. Karimi Abadchi, J., Rezaei, Z., Knöpfel, T., McNaughton, B. L., & Mohajerani, M. H. (2023, January 16). Inhibition is a prevalent mode of activity in the neocortex around awake hippocampal ripples in mice. *eLife, 12*, e79513. https://doi.org/10.7554/eLife.79513
21. Marvin, J. S., Shimoda, Y., Magloire, V., Leite, M., Kawashima, T., Jensen, T. P., ... & Looger, L. L. (2019). A genetically encoded fluorescent sensor for in vivo imaging of GABA. *Nature Methods, 16*(8), 763–770. https://doi.org/10.1038/s41592-019-0469-0

628 22. Rezaei, E., Tohidi, S., Nazari, M., & Karimi Abadchi, J. (2025). Characterization of
629 iGABASnFR2 for in vivo mesoscale imaging of intracortical GABA dynamics.
630 Neurophotonics, 12(3), 035006. https://doi.org/10.1117/1.NPh.12.3.035006
631 23. Yardeni, T., Eckhaus, M., Morris, H. D., Huizing, M., & Hoogstraten-Miller, S. (2011).
632 Retro-orbital injections in mice. *Lab Animal, 40*(5), 155–160.
633 https://doi.org/10.1038/laban0511-155
634 24. Chan, K. Y., Jang, M. J., Yoo, B. B., Greenbaum, A., Ravi, N., Wu, W.-L., Sánchez-
635 Guardado, L., Lois, C., Mazmanian, S. K., Deverman, B. E., & Gradinaru, V. (2017).
636 Engineered AAVs for efficient noninvasive gene delivery to the central and peripheral
637 nervous systems. Nature Neuroscience, 20(8), 1172–1179.
638 https://doi.org/10.1038/nn.4593
639 25. Mohajerani, M. H., Chan, A. W., Mohsenvand, M., LeDue, J., Liu, R., McVea, D. A.,
640 Boyd, J. 819 D., Wang, Y. T., Reimers, M., & Murphy, T. H. (2013). Spontaneous
641 cortical activity alternates 820 between motifs defined by regional axonal projections.
642 Nature Neuroscience, 16(10), 1426–821 1435. https://doi.org/10.1038/nn.3499
643 26. Vanni, M. P., & Murphy, T. H. (2014). Mesoscale transcranial spontaneous activity
644 mapping in GCaMP3 transgenic mice reveals extensive reciprocal connections between
645 areas of somatomotor cortex. Journal of Neuroscience, 34(48), 15931–15946.
646 https://doi.org/10.1523/JNEUROSCI.1818-14.2014
647 27. Silasi, G., Xiao, D., Vanni, M. P., Chen, A. C. N., & Murphy, T. H. (2016). Intact skull
648 chronic 813 windows for mesoscopic wide-field imaging in awake mice. Journal of
649 Neuroscience Methods, 814 267, 141–149.
650 https://doi.org/10.1016/j.jneumeth.2016.04.012

28. Xiao, D., Forys, B. J., Vanni, M. P., & Murphy, T. H. (2021). MesoNet allows automated scaling and segmentation of mouse mesoscale cortical maps using machine learning. Nature 1092 Communications, 12(1). https://doi.org/10.1038/s41467-021-26255-2

29. Kramer, R. H., & Levitan, H. (1979). Cerebral cortical microfluorometry at isosbestic wavelengths for correction of vascular artifact. Science, 205(4407), 693–696. https://doi.org/10.1126/science.223243

30. Ma, Y., Shaik, M. A., Kim, S. H., Kozberg, M. G., Thibodeaux, D. N., Zhao, H. T., Yu, H., & Hillman, E. M. C. (2016). Wide field optical mapping of neural activity and brain haemodynamics: Considerations and novel approaches. Philosophical Transactions of the Royal Society B: Biological Sciences, 371(1705), 20150360. https://doi.org/10.1098/rstb.2015.0360

31. Scott, B. B., Thiberge, S. Y., Guo, C., Brody, C. D., Karpova, A. Y., & Tank, D. W. (2018). 1048 Imaging cortical dynamics in GCaMP transgenic rats with a head-mounted widefield macroscope. Neuron, 100(5), 1045–1058.e5. https://doi.org/10.1016/j.neuron.2018.09.050

32. Syeda, A., Zhong, L., Tung, R., Long, W., Pachitariu, M., & Stringer, C. (2024). Facemap: A framework for modeling neural activity based on orofacial tracking. Nature Neuroscience, 27(1), 1058 187–195. https://doi.org/10.1038/s41593-023-01490-6

33. Buzsáki, G. (2015). Hippocampal sharp wave–ripple: A cognitive biomarker for episodic memory and planning. *Hippocampus, 25*(10), 1073–1188. https://doi.org/10.1002/hipo.22488

34. Wilson, M. A., & McNaughton, B. L. (1994). Reactivation of hippocampal ensemble memories during sleep. *Science, 265*(5172), 676–679. https://doi.org/10.1126/science.8036517

35. Peyrache, A., Khamassi, M., Benchenane, K., Wiener, S. I., & Battaglia, F. P. (2009). Replay of rule-learning related neural patterns in the prefrontal cortex during sleep. *Nature Neuroscience, 12*(7), 919–926. https://doi.org/10.1038/nn.2337
36. Jadhav, S. P., Kemere, C., German, P. W., & Frank, L. M. (2012). Awake hippocampal sharp-wave ripples support spatial memory. *Science, 336*(6087), 1454–1458. https://doi.org/10.1126/science.1217230
37. Buzsáki, G. (1989). Two-stage model of memory trace formation: A role for "noisy" brain states. *Neuroscience, 31*(3), 551–570. https://doi.org/10.1016/0306-4522(89)90423-5
38. Ego-Stengel, V., & Wilson, M. A. (2009). Disruption of ripple-associated hippocampal activity during rest impairs spatial learning in the rat. *Hippocampus, 20*(1), 1–10. https://doi.org/10.1002/hipo.20707
39. Girardeau, G., Benchenane, K., Wiener, S. I., Buzsáki, G., & Zugaro, M. B. (2009). Selective suppression of hippocampal ripples impairs spatial memory. *Nature Neuroscience, 12*(10), 1222–1223. https://doi.org/10.1038/nn.2384
40. Mohajerani, M. H., McVea, D. A., Fingas, M., & Murphy, T. H. (2010). Mirrored bilateral slow-wave cortical activity within local circuits revealed by fast bihemispheric voltage-sensitive dye imaging in anesthetized and awake mice. Journal of Neuroscience, 30(10), 3745–3751. https://doi.org/10.1523/JNEUROSCI.4423-09.2010
41. Lee, S.-H., & Dan, Y. (2012). Neuromodulation of brain states. *Neuron, 76*(1), 209–222. https://doi.org/10.1016/j.neuron.2012.09.012
42. McGinley, M. J., Vinck, M., Reimer, J., Batista-Brito, R., Zagha, E., Cadwell, C. R., Tolias, A. S., Cardin, J. A., & McCormick, D. A. (2015). Waking state: Rapid variations modulate neural and behavioral responses. *Neuron, 87*(6), 1143–1161. https://doi.org/10.1016/j.neuron.2015.09.012

43. Gentet, L. J., Kremer, Y., Taniguchi, H., Huang, Z. J., Staiger, J. F., & Petersen, C. C. H. (2012). Unique functional properties of somatostatin-expressing GABAergic neurons in mouse barrel cortex. *Nature Neuroscience, 15*(4), 607–612. https://doi.org/10.1038/nn.3051

44. Niethard, N., Ngo, H.-V. V., Ehrlich, I., & Born, J. (2018). Cortical circuit activity underlying sleep slow oscillations and spindles. *Proceedings of the National Academy of Sciences of the United States of America, 115*(39), E9220–E9229. https://doi.org/10.1073/pnas.1805517115

45. Zielinski, M. R., Atochin, D. N., McNally, J. M., McKenna, J. T., Huang, P. L., Strecker, R. E., & Gerashchenko, D. (2019). Somatostatin+/nNOS+ neurons are involved in delta electroencephalogram activity and cortical-dependent recognition memory. *Sleep, 42*(10), zsz143. https://doi.org/10.1093/sleep/zsz143

46. Niethard, N., Hasegawa, M., Itokazu, T., Oyanedel, C. N., Born, J., & Sato, T. R. (2016). Sleep-stage-specific regulation of cortical excitation and inhibition. *Current Biology, 26*(20), 2739–2749. https://doi.org/10.1016/j.cub.2016.08.035

47. Desrosiers, J., & Basha, D. (2023). Cortical inhibition, plasticity, and sleep. *The Journal of Neuroscience, 43*(4), 523–525. https://doi.org/10.1523/JNEUROSCI.1631-22.2022

48. Tossell, K., Yu, X., Giannos, P., Anuncibay Soto, B., Nollet, M., Yustos, R., Miracca, G., Vicente, M., Miao, A., Hsieh, B., Ma, Y., Vyssotski, A. L., Constandinou, T., Franks, N. P., & Wisden, W. (2023). Somatostatin neurons in prefrontal cortex initiate sleep-preparatory behavior and sleep via the preoptic and lateral hypothalamus. *Nature Neuroscience, 26*(10), 1805–1819. https://doi.org/10.1038/s41593-023-01430-4

49. Nazari, M., Abadchi, J. K., Naghizadeh, M., Bermudez-Contreras, E. J., McNaughton, B. L., Tatsuno, M., & Mohajerani, M. H. (2023). Regional variation in cholinergic terminal activity determines the non-uniform occurrence of cortical slow waves during REM sleep in mice. Cell Reports, 42(5), 112450. https://doi.org/10.1016/j.celrep.2023.112450

50. Opalka, A. N., Huang, W., Liu, J., Liang, H., & Wang, D. V. (2020). Hippocampal ripple coordinates retrosplenial inhibitory neurons during slow-wave sleep. *Cell Reports, 30*(2), 432–441.e3. https://doi.org/10.1016/j.celrep.2019.12.038

51. Alexander AS, Rangel LM, Tingley D, Nitz DA (2018). Neurophysiological signatures of temporal coordination between retrosplenial cortex and the hippocampal formation. Behavioral Neuroscience, 132(6), 453–468. https://doi.org/10.1037/bne0000254

52. Wang DV, Ikemoto S (2016). *Coordinated interaction between hippocampal sharp-wave ripples and anterior cingulate unit activity*. The Journal of Neuroscience, 36(41), 10663–10672. https://doi.org/10.1523/JNEUROSCI.1042-16.2016

53. Atallah, B. V., & Scanziani, M. (2009). Instantaneous modulation of gamma oscillation frequency by balancing excitation with inhibition. *Neuron, 62*(4), 566–577. https://doi.org/10.1016/j.neuron.2009.04.027

54. Okun, M., & Lampl, I. (2008). Instantaneous correlation of excitation and inhibition during ongoing and sensory-evoked activities. *Nature Neuroscience, 11*(5), 535–537. https://doi.org/10.1038/nn.2105

Figure legends

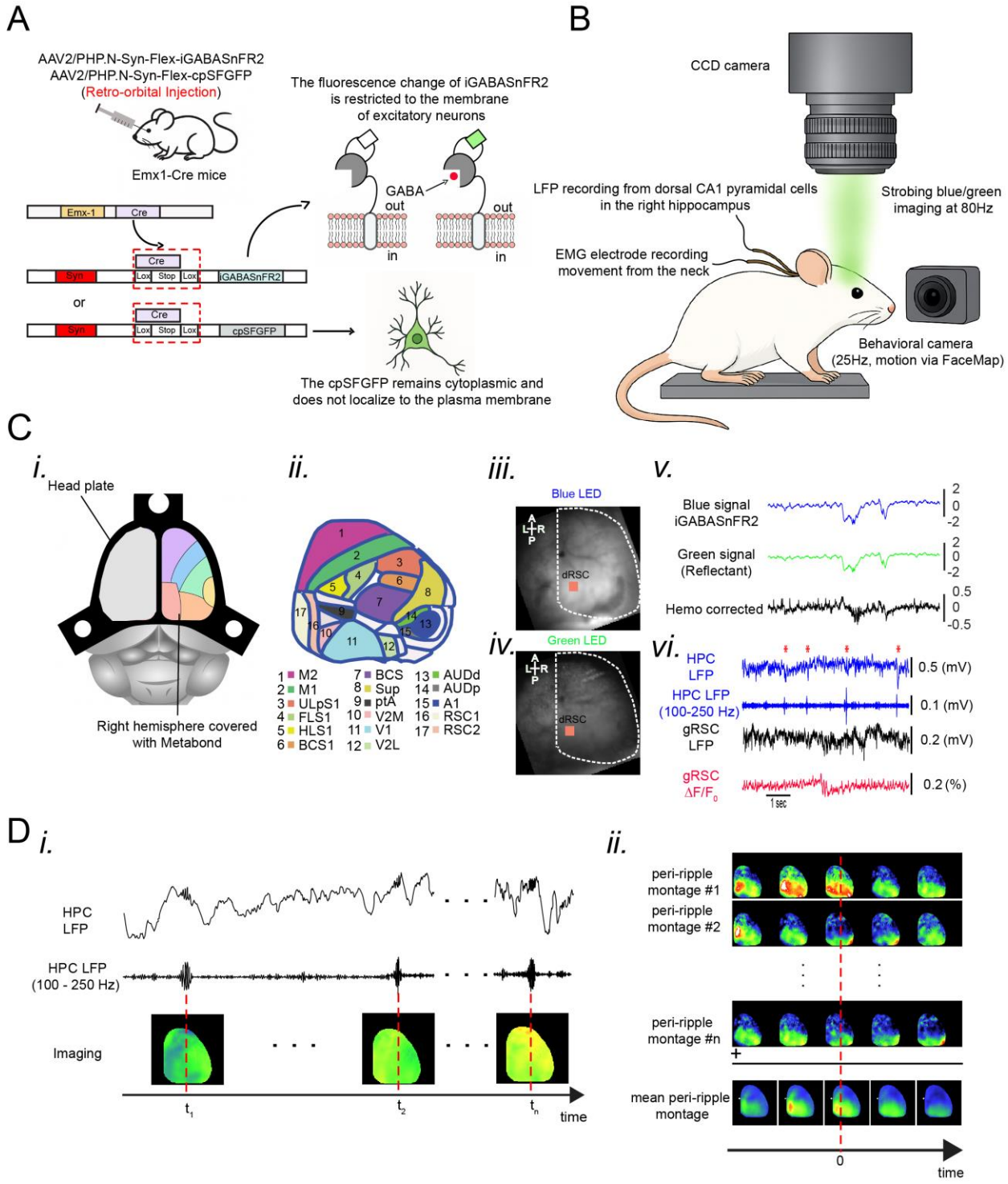

Figure 1. Experimental protocol for imaging neocortical GABA dynamics during sleep and hippocampal ripples. (A) Schematic of viral delivery and genetic targeting. Emx1-Cre mice received retro-orbital injections of either AAV2/PHP.eB-Syn-Flex-iGABASnFR2 or AAV2/PHP.eB-Syn-Flex-cpSFGFP as a control. In Emx1-Cre mice, Cre recombinase drives expression of the GABA sensor iGABASnFR2 or control construct specifically in cortical excitatory neurons. iGABASnFR2 is membrane-bound and reports extracellular GABA binding

via fluorescence increases, whereas cpSFGFP is cytosolic and does not respond to GABA. (B) Diagram of the in vivo imaging and recording setup. A CCD camera captures widefield fluorescence from the dorsal cortex through a cranial window. Imaging is synchronized to alternating blue (470 nm) and green (530 nm) LED strobes at 80 Hz for excitation of iGABASnFR2 and collection of reflectance signals, respectively. Simultaneous recordings include hippocampal LFPs from dorsal CA1 to detect SWRs, neck EMG for movement and arousal state, and a behavioral camera (25 Hz) for motion tracking via FaceMap. (C) Imaging coverage and signal correction. (i)Schematic showing the imaging configuration: the right hemisphere was exposed for imaging which was sealed it with Metabond, while the left hemisphere remained intact. (ii) Schematic showing the 17 identified cortical regions used in ROI-based analyses. (iii–iv) Example cortical images under blue and green LED illumination. The red box marks the dorsal retrosplenial cortex (dRSC), one of the key analysis regions. (v) Traces from the same site showing raw iGABASnFR2 fluorescence (blue), reflectance (green), and the hemodynamically corrected signal (black). (vi) Example traces showing simultaneous hippocampal LFPs (broadband and ripple-filtered), local dRSC LFP, and corrected GABA fluorescence from dRSC. Detected SWRs are aligned with both GABA and LFP signals. (D) Alignment and averaging of peri-ripple GABA activity. (i) Example SWRs from the ripple-band filtered LFP (100–250 Hz) are aligned with concurrent widefield GABA imaging frames. (ii) For each detected SWR, peri-event GABA imaging frames are extracted, aligned to the ripple center (t = 0), and assembled into individual montages. Mean peri-ripple maps are generated across events to characterize spatiotemporal GABA dynamics around SWRs.

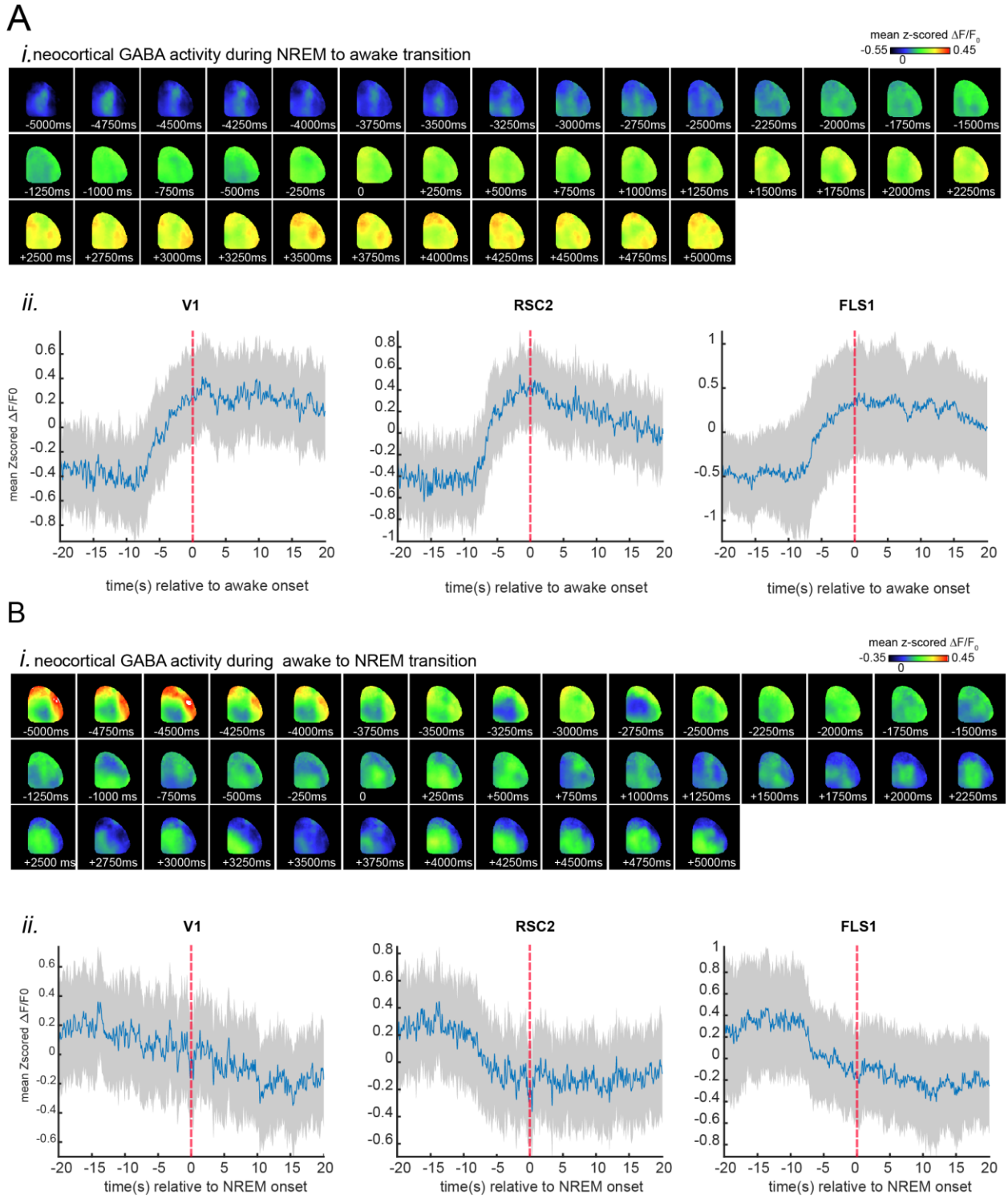

Figure 2. Neocortical GABA activity during NREM is used to awaken and awaken NREM transitions. (A) Transition from NREM to Awake. (i) Representative montage of mean neocortical GABA activity during wake-NREM transition recorded with the GABA-sensing fluorescent reporter iGABASnFR2. Images present 5-second time bins, and zero s-time marks wake onset. Data were scaled and z-scored to the shown color bars (n=5). (ii) Representative

sample traces of iGABASnFR2 signals from regions indicated in (i). The plots present the mean optical signals recorded in 3 × 3-pixel boxes (~0.04 mm^2) throughout cortical regions. Width of shading surrounding each plot indicates standard error of the mean (SEM). The time 0 s indicates wake onset. (B) Transition from Awake to NREM. (i) Representative montage of mean neocortical GABA activity during wake-NREM transition. Images present 5-second time bins, and zero s-time marks NREM onset. Data were scaled and z-scored to the shown color bars (n=5). (ii) Representative sample traces of iGABASnFR2 signals from regions indicated in (i). The plots present the mean optical signals recorded in 3 × 3-pixel boxes (~0.04 mm^2) throughout cortical regions. Shaded areas surrounding each trace indicate reproducibility, which is confirmed. The time 0 s indicates NREM sleep onset.

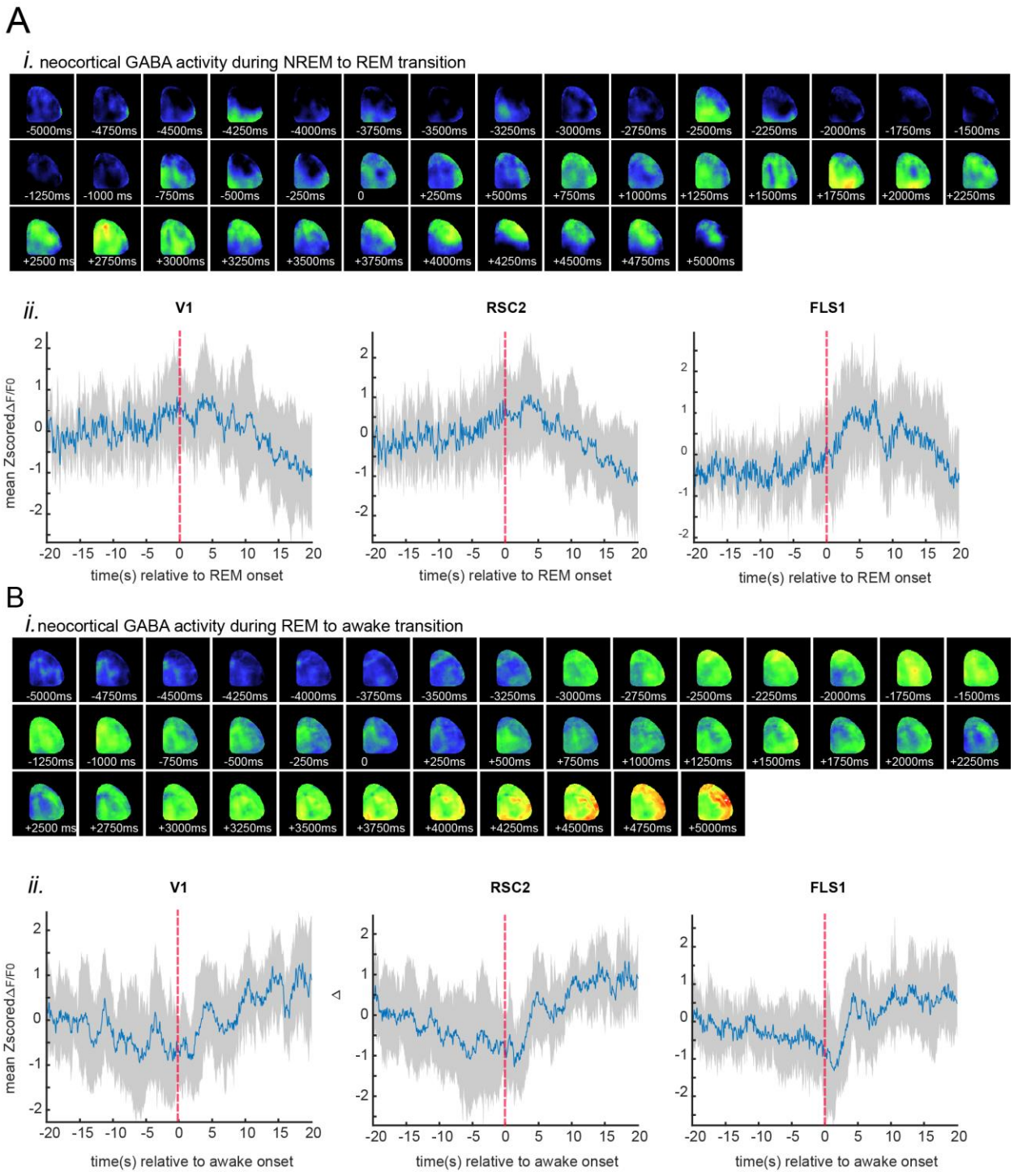

Figure 3. Neocortical GABA Activity During NREM to REM and REM to Awake Transitions. (A) Transition to REM. (i) Montage of mean neocortical GABA activity recorded using the GABA-sensing fluorescent reporter iGABASnFR2 during natural sleep. Images represent 5-second epochs, and zero s-time represents REM onset. Data were z-scored and normalized to the color bars shown (n=5). (ii) Representative traces of iGABASnFR2 signals from regions marked in (i) in an exemplary animal. The plots show the mean optical signals recorded in 3 × 3-pixel boxes (~0.04 mm²) within the visual (V1), retrosplenial (RSC), and forelimb

794 somatosensory (FLS1; magenta) cortices. The thickness of the shading around each plot gives the
795 SEM. The time 0 s represents REM onset. (B) Transition to wake at wake-onset. (i) Montage of
796 mean neocortical GABA activity recorded using the GABA-sensing fluorescent reporter
797 iGABASnFR2 during wake-onset transition from REM. Images represent 5-second epochs, and
798 zero s-time represents wake-onset. Data were z-scored and normalized to the color bars shown
799 (n=5). (ii) Representative traces of iGABASnFR2 signals from regions marked in (i) in an
800 exemplary animal. The plots show the mean optical signals recorded in 3 × 3-pixel boxes (~0.04
801 mm^2) within the visual (V1), retrosplenial (RSC2), and forelimb somatosensory (FLS1; magenta)
802 cortices. The thickness of the shading around each plot gives the SEM. The time 0 s represents
803 wake-onset.

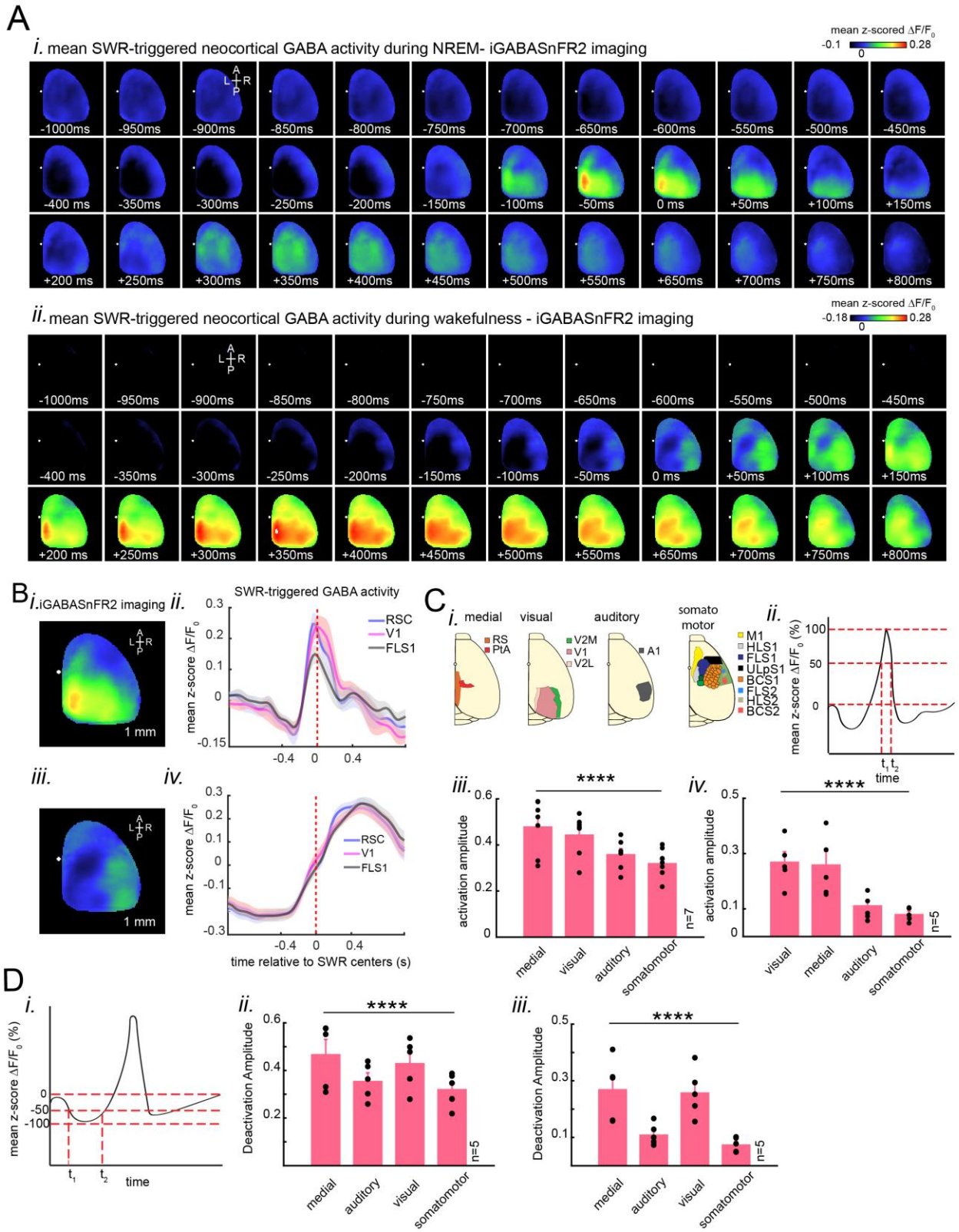

Figure 4. Peri-SWR neocortical GABA activity: activation and deactivation patterns across sleep and wake states. (A) Characteristic montage of mean peri-SWR neocortical GABA activity,

as visualized with the GABA-sensing fluorescent reporter iGABASnFR2, during head-restrained natural sleep (i) and wakefulness (ii). Time 0 marks SWR centers. Images z-scored and scaled to respective color bars. (B) (i–iv) Sample traces of iGABASnFR2 signals. Panels (Bi, Bii) show natural sleep traces, and (Biii, Biv) show wake traces, taken from sample regions in panels (Ai) and (Aii). Traces show mean optical signals from 3 × 3-pixel boxes (~0.04 mm^2) within retrosplenial (blue), visual (black), and forelimb somatosensory (magenta) cortices. Shaded areas around regions of each plot are SEM. SWR centers mark time 0. (C) (i) Four large neocortical subnetworks (medial, visual, auditory, and somatomotor), structurally delimited. (ii) Quantification of activation amplitude schema, defined as mean within-whole-width-at-half-maximum (t1 to t2) of the mean. (iv–v) Grand average (n = 7 animals) of activation amplitudes across subnetworks during wake and sleep, ordered in decreasing order. Each data point represents average activation amplitude for all regions within a subnetwork for one animal. Statistical Analysis: Awake data had a significant subnetwork influence ($F(3,18) = 30.051$, $p = 3.18 \times 10^{-7}$, Greenhouse-Geisser adjusted $p = 7.03 \times 10^{-5}$), and post-hoc differences were found between auditory and medial ($p = 0.0075$), auditory and visual ($p = 0.0025$), medial and somatomotor ($p = 0.0027$), and somatomotor and visual ($p = 0.0053$). Sleep data also revealed a significant subnetwork effect ($F(3,12) = 21.608$, $p = 3.96 \times 10^{-5}$, Greenhouse-Geisser corrected $p = 0.0017$), with posthoc differences between auditory and medial ($p = 0.0305$), auditory and visual ($p = 0.0146$), and medial and somatomotor ($p = 0.0366$). (D) (i–iii) neocortical deactivations preceding SWRs. (Di, Dii) show results for wakefulness and sleep, respectively. Deactivation amplitudes were rectified for group comparison, with higher values indicating more substantial deactivation. Bar plots depict mean ± SEM. Statistical Analysis: Awake data recorded a significant subnetwork effect ($F(3,12) = 13.869$, $p = 0.00033$, Greenhouse-Geisser corrected $p = 0.0047$), and posthoc differences between auditory and visual ($p = 0.032$), medial and somatomotor ($p = 0.041$), and visual and somatomotor ($p = 0.061$) regions. Sleep data recorded a significant subnetwork effect ($F(3,12) = 21.608$, $p = 3.96 \times 10^{-5}$, Greenhouse-Geisser corrected $p = 0.0017$), and posthoc differences between auditory and visual ($p = 0.015$), auditory and medial ($p = 0.031$), and somatomotor and visual ($p = 0.010$) regions. There are five supplementary panels in the figure.

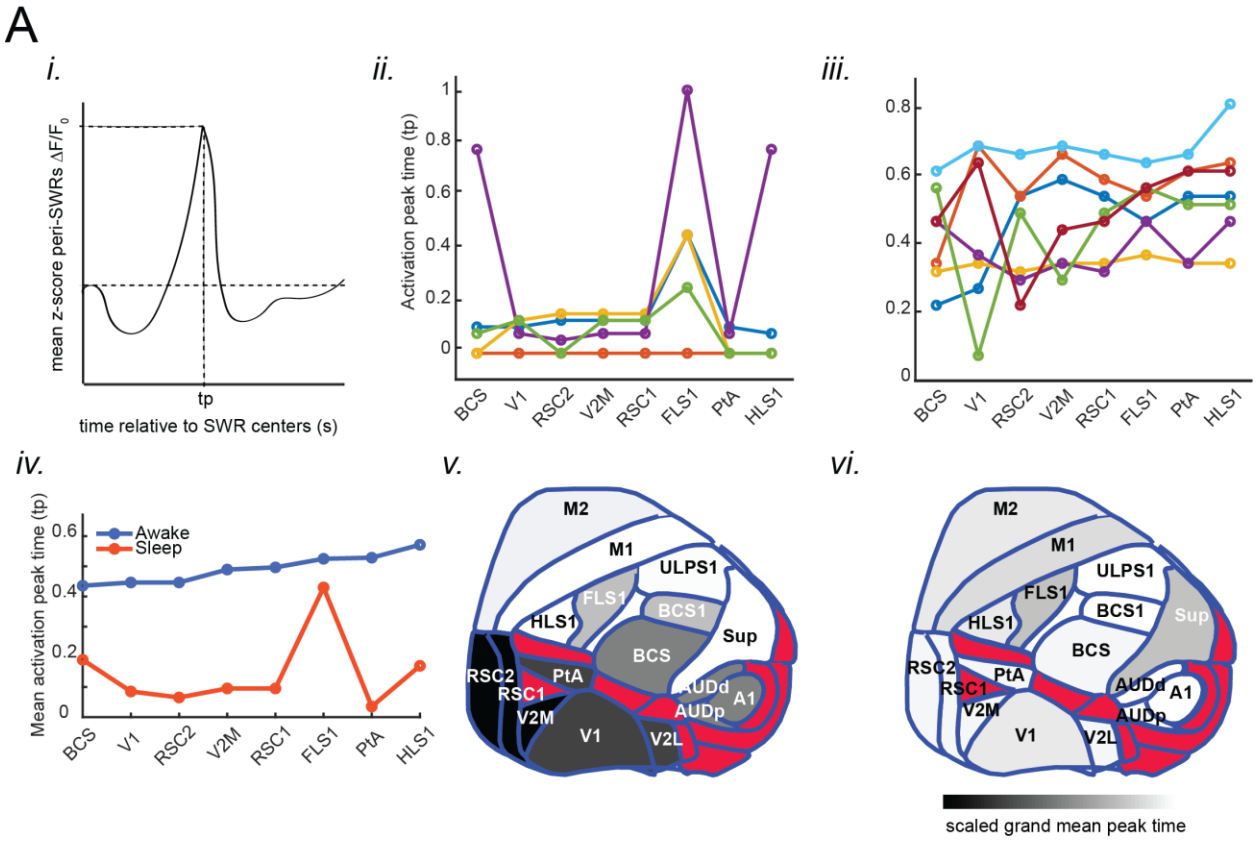

Figure 5. Cortical regions exhibit state-dependent peak GABA activation dynamics around SWRs during natural sleep and wakefulness. (A) (i) Peak GABA activation time (tp) for peri-SWR in each cortical region was determined as peak time of mean peri-SWR GABA activity trace (blue trace) and provides an index of peak GABA activation time relative to center of SWR. (ii) Sleep Condition: Repeated-measures ANOVA revealed significant regional variation in tp ($F(10,40) = 5.0973$, $p = 8.9111e{-}05$). A statistically significant positive linear trend (slope=0.011273 s/region,p=0.047249) discloses medial-to-lateral progression of tp during sleep, consistent with a subtle medial-to-lateral propagation of GABA activation. (iii) Awake Condition: Repeated-measures ANOVA revealed strong and statistically significant regional variation in tp ($F(10,60) = 20.156$, $p = 1.116e{-}15$). Post-hoc linear trend analysis confirmed a statistically significant positive slope (slope=0.02724 s/region, p=0.024326), which discloses a consistent and systemicdelayed,tp from medial toward lateral regions in wake stage. (iv) Post-hoc Linear Trend Analysis: Linear trend analysis confirmed state-dependent dynamics. In wake, a statistically significant positive slope (0.02724 s/region=0.024326) discloses a robust medial-to-lateral gradient. In sleep, a negligibly but statistically significant smaller slope (0.011273 s/region=0.047249) reveals less strenuous regional variations. The corresponding graph reveals the result, which shows steep and consistent regional variation in awake data compared with sleep. (v) Spatial maps during sleep (n=5) reveal higher earlier peak tp in medial regions like RSC1, RSC2, and PtA, and subsequent lateral propagation of activation. The result discloses an orchestrated medial-to-lateral propagation of GABAergic activation during natural sleep. (vi) Spatial maps for wakefulness (n=7) indicate delayed activation in medial regions and a more homogeneous distribution of tp values throughout cortical regions. The pattern indicates characteristic cortical dynamics in wakefulness, with a strong medial-to-lateral gradient in GABA activation timing.

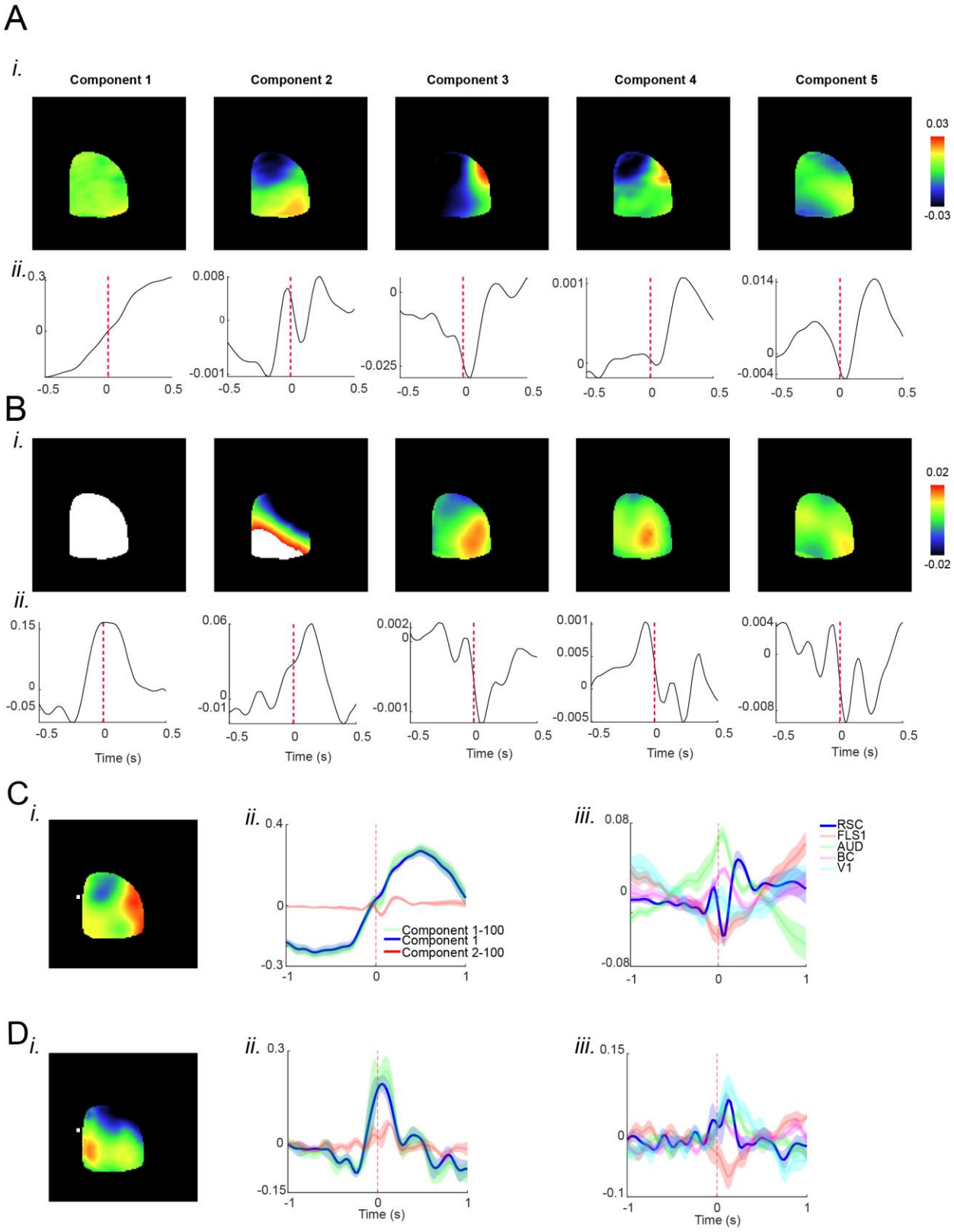
A
i.
Component 1
Component 2
Component 3
Component 4
Component 5
0.03
-0.03
ii.
B
i.
0.02
-0.02
ii.
Time (s)
C
i.
ii.
Component 1-100
Component 1
Component 2-100
iii.
RSC
FLS1
AUD
BC
V1
D
i.
ii.
Time (s)
iii.
Time (s)

860

Figure 6. Spatial and Temporal Modes of Peri-Ripple iGABASnFR2 Activity and Region-Specific Dynamics. (A, B) Spatial (i) and temporal (ii) modes of the five largest singular components of the peri-ripple combined iGABASnFR2 activity stack in wakeful (A) and sleep (B) epochs. Spatial mode of first component exhibits absence of sharp topographical features, consistent with a widespread increase of the iGABASnFR2 signal following the ripple, which overwhelms the entire GABA signal and corresponding temporal mode. This overall response is invariant across states, with the temporal amplitude of the first component being one order of magnitude larger than the others, thus revealing its predominance in describing the dynamics of global peri-ripple GABA activity.Components 2–5 demonstrate state-dependent differences in the spatiotemporal structure of GABA activity. When awake (A), spatial maps of Components 2–5 illustrate localized GABA activity, with particularly strong activity in sensory areas like the barrel cortex (BC) and visual cortex (V1). Their temporal profiles reveal rapid, sharp peaks at fixed times of ripple initiation, which can be resolved as specific and region-specific GABAergic control. Asleep (B), spatial modes of Components 2–5 reveal less spatially localized patterns of increased associative area activity (e.g., retrosplenial cortex, RSC) and decreased sensory area activity—corresponding temporal profiles asleep reveal slower dynamics, and bear no such sharp peaks as during wakefulness. (C, D) Peri-ripple regional GABA activity reconstructed for significant regions of interest (ROIs)—the retrosplenial cortex (RSC), barrel cortex (BC), visual cortex (V1), auditory cortex (AUD), and forelimb somatosensory cortex (FLS1)—reveal state-dependent peri-ripple dynamics. These findings have considerable implications for our understanding of brain activity in wakefulness and sleep. Awake (C), BC and V1 reveal well-defined and high-amplitude peaks in their temporal profiles (Cii), and statistical comparison (Ciii) reveals significantly increased sensory responses as compared to RSC. When asleep (D), GABA activity is more diffusely distributed across areas, with RSC standing out as the predominant area with prolonged and sizable activity. Sensory areas like BC and V1 have weakened responses when asleep (Dii). Shading in temporal profiles (Cii, Dii) denotes the SEM and statistical comparison (Diii) emphasizes the relative enhancement of RSC activity with respect to sensory areas when asleep. Shading around these profiles also denotes the SEM.